Improved Parameter-Estimation With MRI-Constrained PET Kinetic Modeling: A Simulation Study

Kjell Erlandsson, Maria Liljeroth, David Atkinson, Simon Arridge, Sebastien Ourselin, and Brian F. Hutton, *Senior Member, IEEE*

***Abstract*—Kinetic analysis can be applied both to dynamic PET and dynamic contrast enhanced (DCE) MRI data. We have investigated the potential of MRI-constrained PET kinetic modeling using simulated [^{18}F]2-FDG data for skeletal muscle. The volume of distribution, V_e, for the extra-vascular extra-cellular space (EES) is the link between the two models: It can be estimated by DCE-MRI, and then used to reduce the number of parameters to estimate in the PET model. We used a 3 tissue-compartment model with 5 rate constants (3TC5k), in order to distinguish between EES and the intra-cellular space (ICS). Time-activity curves were generated by simulation using the 3TC5k model for 3 different V_e values under basal and insulin stimulated conditions. Noise was added and the data were fitted with the 2TC3k model and with the 3TC5k model with and without V_e constraint. One hundred noise-realisations were generated at 4 different noise-levels. The results showed reductions in bias and variance with V_e constraint in the 3TC5k model. We calculated the parameter k_3'', representing the combined effect of glucose transport across the cellular membrane and phosphorylation, as an extra outcome measure. For k_3'', the average coefficient of variation was reduced from 52% to 9.7%, while for k_3 in the standard 2TC3k model it was 3.4%. The accuracy of the parameters estimated with our new modeling approach depends on the accuracy of the assumed V_e value. In conclusion, we have shown that, by utilising information that could be obtained from DCE-MRI in the kinetic analysis of [^{18}F]2-FDG-PET data, it is in principle possible to obtain better parameter estimates with a more complex model, which may provide additional information as compared to the standard model.**

***Index Terms*—FDG, kinetic modeling, PET/MRI.**

Manuscript received July 15, 2015; revised October 02, 2015; accepted December 04, 2015. This work was supported by the EPSRC under Grant EP/K005278/1. UCL/UCLH research is supported by the NIHR Biomedical Research Centers funding scheme.

K. Erlandsson is with the Institute of Nuclear Medicine, University College London, London WC1E 6BT, U.K. (e-mail: k.erlandsson@ucl.ac.uk).

M. Liljeroth was with the Institute of Nuclear Medicine, University College London, London WC1E 6BT, U.K. She is now with University Hospital Southampton, Southampton SO16 6YD, U.K.

D. Atkinson is with the Centre for Medical Imaging, University College London, London WC1E 6BT, U.K.

S. Arridge is with the Department of Computer Science, University College London, London WC1E 6BT, U.K.

S. Ourselin is with the Centre for Medical Image Computing, University College London, London WC1E 6BT, U.K.

B. F. Hutton is with the Institute of Nuclear Medicine, University College London, London WC1E 6BT, U.K., and also with the Centre for Medical Radiation Physics, University of Wollongong, Wollongong NSW 2522, Australia.

Digital Object Identifier 10.1109/TNS.2015.2507444

I. Introduction

KINETIC analysis of dynamic PET can be used for estimation of various physiological or biochemical parameters (see [1]–[4] for general summaries and [5][6] for FDG). The models used in these analyses are simplified versions of the true physiological and biochemical processes involved. Simplification is needed for reasons of numerical stability of the estimated parameters. Also dynamic MRI data can be used for estimation of physiological parameters. We wish to extend and improve the stability of conventional PET modeling through the use of specific kinetic MRI parameters. The reason behind this investigation is the recent introduction of combined PET/MRI scanners, which allow for simultaneous acquisition of PET and MRI data [7].

In dynamic contrast enhanced (DCE) MRI studies, Gd-based contrast agents can diffuse across the capillary walls but not across the cellular membrane. The data can be analysed using a model with one tissue-compartment (TC) and two rate constants, as shown in Fig. 1 [8]. We will refer to this model as a 1TC2k-model. The rate constants for forward and reverse transfer between blood and tissue are conventionally called K^{trans} and k_{ep}, respectively, and their ratio is the volume of distribution of the extra-vascular extra-cellular space (EES) ($V_e = K^{trans}/k_{ep}$) [8].

In PET studies, the most commonly used tracer is ^{18}F-labelled 2-fluoro-2-deoxy-D-glucose ([^{18}F]2-FDG). This is a glucose analogue, which can be used for measuring the metabolic rate of glucose (MR_{glu}). Most clinical [^{18}F]2-FDG studies consist of a single static PET scan, performed some time after the injection of the tracer. However, more accurate uptake values can be obtained by performing a dynamic scan and kinetic analysis.

After injection, [^{18}F]2-FDG is carried by the blood stream to different organs and tissues in the body. The tracer is extracted from the vascular to the extra-vascular space in the same way as glucose. In skeletal muscle this occurs by diffusion [9]. It is then transported from the EES across the cellular membrane to the intra-cellular space (ICS). This transport is facilitated by glucose transporters, some of which are insulin mediated [9]. Inside the ICS, [^{18}F]2-FDG can be phosphorylated to [^{18}F]2-FDG-6-PO_4 by the enzyme hexokinase. Phosphorylation is also the first step in the metabolism of glucose, but

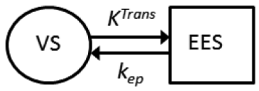

Fig. 1. DCE-MRI model with vascular space (VS) and extra-vascular extra-cellular space (EES).

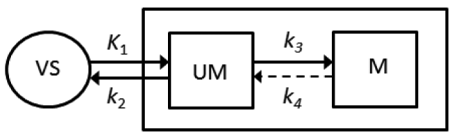

Fig. 2. Standard [^{18}F]2-FDG model with two tissue-compartments, representing un-metabolised (UM) and metabolised (M) tracer, respectively.

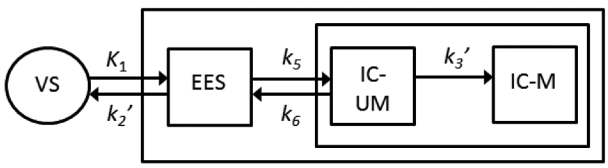

Fig. 3. [^{18}F]2-FDG model for skeletal muscle, proposed by Bertoldo et al. [10], including one EES compartment and two ICS compartments for un-metabolised (IC-UM) and metabolised tracer (IC-M), respectively. NB: The symbols for the rate constants are different from those in [10].

[^{18}F]2-FDG does not go any further along this metabolic pathway. In some tissues (e.g. brain), [^{18}F]2-FDG-6-PO_4 can be dephosphorylated back to [^{18}F]2-FDG by the enzyme glucose-6-phosphatase. This enzyme is not present in skeletal muscle and therefore no dephosphorylation occurs [9]. Free [^{18}F]2-FDG can be transported back across the cellular membrane to the EES and from there back to the blood stream.

Kinetic analysis of dynamic [^{18}F]2-FDG PET data was first applied to brain studies, and two different models were developed at an early stage: An irreversible model with 3 rate constants was proposed by Sokoloff *et al.* in 1977 [3], and a reversible model with 4 rate constants by Phelps *et al.* in 1979 [4] (see Fig. 2). Both models have two TCs, and we will refer to them as the 2TC3k and 2TC4k model, respectively. The parameter k_4 was introduced to represent dephosphorylation, which in the 2TC3k model, is assumed to be negligible. In the 2TC4k model, dephosphorylation is assumed to occur, although at a rate much lower than that of phosphorylation ($k_4 \ll k_3$). Neither of these models distinguish between the EES and the ICS, which corresponds to the implicit assumption that the rate of transport across the cellular membrane is much faster than the rate of phosphorylation, as this would lead to a steady state in the [^{18}F]2-FDG concentrations in EES and ICS from an early time point in the experiment.

In 2001, Bertoldo *et al.* proposed a model with 3 TCs and 5 rate-constants (3TC5k) for studying uptake of [^{18}F]2-FDG in skeletal muscle (Fig. 3) [10]. They argued that the transport of [^{18}F]2-FDG across the cellular membrane in skeletal muscle was not fast enough for the assumption mentioned above. This model is more realistic, containing one compartment for the EES and two for the ICS, for un-metabolised and metabolised tracer, respectively. However, with 5 parameters to estimate, there can be problems of parameter identifiability and numerical instability with noisy data.

In 2006, Bertoldo *et al.* presented a study, which combined the use of [^{18}F]2-FDG and the nonphosphorylatable glucose analog ^{11}C-labeled 3-O-methyl-D-glucose [^{11}C]3-OMG [11]. The data from the former tracer was analysed using the 3TC5k model mentioned above, while a 2TC4k model was used for the latter tracer. The purpose of this study was to investigate the effect of insulin on the distribution of control among glucose delivery, transport, and phosphorylation in human skeletal muscle. The rate of delivery and transport were obtained from the [^{11}C]3-OMG data, while the rate of phosphorylation was obtained from the [^{18}F]2-FDG data. The authors observed that, under insulin-stimulated conditions, the efficiency of glucose transport was increased by a factor of ~ 6 compared to fasting conditions, and thereby the uptake rate was constrained by the rate of delivery.

Another dual-tracer approach, with a two-injection scanning protocol, was proposed by Huang *et al.* [9] using [^{18}F]2-FDG in combination with the nonphosphorylatable glucose analog ^{18}F-labeled 6-fluoro-6-deoxy-D-glucose ([^{18}F]6-FDG). They used a 3TC5k model in order to resolves the delivery, transport, and phosphorylation steps of the glucose metabolism in skeletal muscle. The model was based on Michaelis–Menten kinetics, so as to utilize information obtained from the competition between glucose and its radiolabeled analogs.

Zhang *et al.* [12] combined [^{15}O]-H_2O PET with DCE-MRI in order to determine maps of the permeability-surface area product (PS) for the MRI contrast agent in tumours.

Here, we propose the use of information derived from DCE-MRI to constrain the kinetic model for [^{18}F]2-FDG PET in order to obtain more robust parameter estimation with a more realistic model. These data sets can be acquired simultaneously using an integrated PET/MRI scanner [7]. The key for linking the two models is the EES compartment, and therefore we need to use a 3TC-model for the PET data. This could also allow for estimation of more specific biological parameters, in addition to the standard parameters, which could be clinically relevant. We have evaluated the potential usefulness of this approach with simulated data for skeletal muscle.

II. Theory

A. Outcome Measures

The main outcome measure in standard [^{18}F]2-FDG PET kinetic analysis is the macro-parameter K_i, which represents the combined effect of delivery, transport and metabolism. This parameter can be determined both with the standard 2TC3k model (Fig. 2):

$$K_i = \frac{K_1 k_3}{k_2 + k_3} \tag{1a}$$

and with the 3TC5k model (Fig. 3):

$$K_i = \frac{K_1 k_5 k_3'}{k_2' k_6 + k_2' k_3' + k_5 k_3'} \tag{1b}$$

This parameter can be obtained directly from the impulse response function describing the system [2]. It corresponds to the

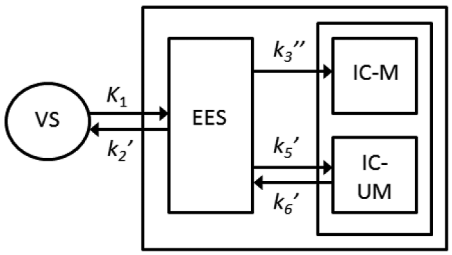

Fig. 4. Uncoupled [^{18}F]2-FDG model including the parameter k_3''.

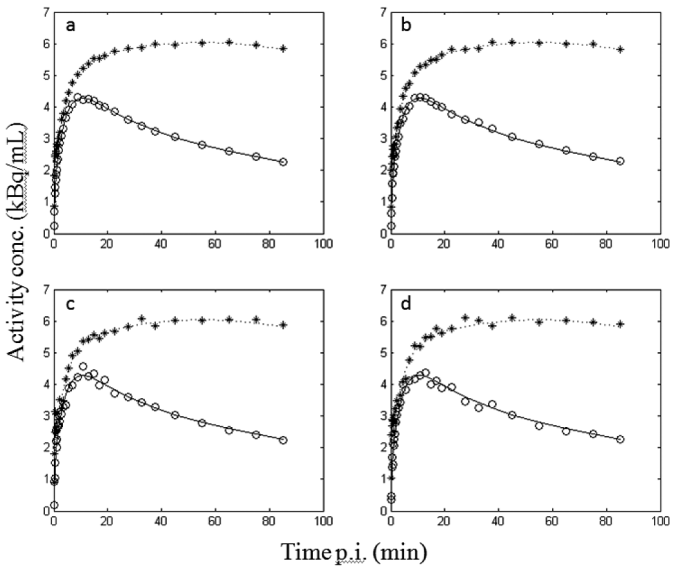

Fig. 5. Examples of simulated TACs with 4 different noise-levels for the basal (solid lines, circles) and insulin (dotted lines, stars) conditions.

rate of uptake of tracer from blood to tissue at steady state and is the basis for calculation of $\mathrm{MR_{glu}}$.

We also define the parameter k_3'', representing the combined effect of transport across the cellular membrane and phosphorylation:

$$k_3'' = \frac{k_5 k_3'}{k_6 + k_3'} \tag{2}$$

The meaning of this parameter can be illustrated by the model in Fig. 4, in which the 2 ICS compartments are uncoupled. k_3'' is similar to k_3 in the standard model, but it is more specific, due to the explicit differentiation between EES and ICS. The models in Figs. 3 and 4 are in practice identical, the difference lies in the interpretation of the parameters. The rate constants of one model can be derived from those of the other one.

B. Volume of Distribution

The concept of "volume of distribution" has a slightly different meaning when used in the context of PET or MRI data. In MRI the term refers to the volume the physical space in which free contrast agent molecules can move around. In PET, the concept has been extended to include both free and bound tracer. The total volume of distribution for a reversible tracer, described by a 2TC4k model, is defined as follows [13]:

$$V_T = \frac{K_1}{k_2}\left(1 + \frac{k_3}{k_4}\right) \tag{3}$$

The two terms correspond to free and bound tracer, respectively. In PET studies, V_T is commonly used as an outcome measure to quantify binding of reversible tracers. It can be interpreted as the volume of plasma required to account for the amount of tracer present in a unit volume of tissue. In this paper, we will use the volume of distribution V_e, referring to the volume of the EES available for diffusion of either free tracer or contrast agent. This parameter is not dependent on extraction, transport or binding of the tracer or contrast agent.

Our basic assumption is that

$$V_e = \frac{K_1}{k_2'} \tag{4}$$

This implies that the transport between the vascular and extravascular spaces is symmetric, but the k_2' parameter is influenced by the tissue-fraction effect, as the concentration of tracer in the EES cannot be measured directly. The same assumption was made by Huang *et al.* [9].

C. New Modeling Approach

We propose the use of the 3TC5k PET model (Fig. 3), constrained by the DCE-MRI estimated V_e value. We have renamed the rate constants with respect to the nomenclature used by Bertoldo *et al.* [5]. The reason for this is that we want the rate constant with index 3 to represent the phosphorylation step, as in the standard model. Also, compared to this model, the new rate constants are the ones representing transport across the cellular membrane, which we therefore name k_5 and k_6. Some of the rate constants in Fig. 3 have been primed in order to distinguish them from rate constants in the standard model with the same index.

In order to use the model, the DCE-MRI data are analysed first, and V_e is estimated and incorporated into the PET model as $k_2' = K_1/V_e$, thereby the number of parameters to estimate is reduced by 1.

For comparison we also used the 3TC5k model without constraint. In this case, V_e was estimated as one of the model parameter and k_2' was obtained as above. This way we could restrict the range of V_e to [0, 1].

III. Materials and Methods

A. Evaluation

To test our new modeling approach, we generated time-activity curves using the 3TC5k model. Data were simulated for 3 different V_e values (0.08, 0.16 and 0.24 mL/mL). The rate constants corresponding to $V_e = 0.08$ were the ones determined experimentally by Bertoldo *et al.* [10], although slightly rounded-off for simplicity. For the other V_e values, a scaling procedure was applied, so that k_2' and k_5 were inversely proportional to V_e, and k_3' and k_6 inversely proportional to $V_i =$

TABLE I
PARAMETER VALUES FOR SIMULATIONS USING THE 3TC5K MODEL UNDER BASAL CONDITIONS

Parameter	*Values*		
V_e	0.08000	0.16000	0.24000
V_b	0.00300	0.00300	0.00300
K_1	0.02800	0.02800	0.02800
k_2'	0.35000	0.17500	0.11667
k_5	0.05000	0.02500	0.01667
k_6	0.04000	0.04382	0.04845
k_3'	0.03000	0.03287	0.03634
K_i	0.00162	0.00162	0.00162

TABLE II
PARAMETER VALUES FOR SIMULATIONS USING THE 3TC5K MODEL UNDER INSULIN STIMULATED CONDITIONS

Parameter	*Values*		
V_e	0.08000	0.16000	0.24000
V_b	0.01500	0.01500	0.01500
K_1	0.02800	0.02800	0.02800
k_2'	0.35000	0.17500	0.11667
k_5	0.15000	0.07500	0.05000
k_6	0.03000	0.03291	0.03644
k_3'	0.06000	0.06582	0.07289
K_i	0.00622	0.00622	0.00622

$(1 - V_e - V_b)$, the volume of distribution of the ICS (V_b is the tissue blood volume). This procedure was based on the tissue fraction effect, mentioned above, resulting in the same K_i for all V_e values. Simulations were done both for basal and insulin stimulated conditions. The parameters used are presented in Tables I–II.

Noise-free time-activity curves (TACs) were generated with the following time-frames: 9×10 and 3×30 s, 3×1, 7×2, 4×5 and 5×10 min, with a total scanning time of 90 min. Normally distributed noise was added to the TACs, with standard deviation (σ) values based on the activity concentration (A) and the frame length (Δt) as follows:

$$\sigma = c\sqrt{A/\Delta t} \tag{5}$$

where c is a proportionality constant, which was changed in order to obtain 4 different noise-levels. One hundred noise-realisations were generated at each noise-level. The data were fitted with the standard 2TC3k model, and with the 3TC5k model, with and without constraint. The mean value and standard deviation of the estimated parameters were calculated across noise-realisations. The data generation and the curve-fitting were done with the software package COMCAT [14] in Matlab R1013a (The Mathworks, Inc., Natick, MA).

TABLE III
ESTIMATED VALUES (mean $\pm$ SD) FOR THE 2TC3K-MODEL WITH $V_e = 0.08$, BASAL CONDITIONS

	Noise level			
	1	*2*	*3*	*4*
K_1	0.02248 ±0.00043	0.02265 ±0.00094	0.02248 ±0.00139	0.02255 ±0.00180
k_2	0.22573 ±0.00527	0.22735 ±0.01146	0.22571 ±0.01748	0.22665 ±0.02236
k_3	0.01968 ±0.00023	0.01965 ±0.00050	0.01966 ±0.00080	0.01964 ±0.00099
K_i	0.00180 ±0.00001	0.00180 ±0.00002	0.00180 ±0.00003	0.00180 ±0.00005

TABLE IV
ESTIMATED VALUES (mean $\pm$ SD) FOR THE UNCONSTRAINED 3TC5K MODEL WITH $V_e = 0.08$, BASAL CONDITIONS

	Noise level			
	1	*2*	*3*	*4*
K_1	0.02814 ±0.00080	0.02855 ±0.00170	0.02852 ±0.00247	0.02862 ±0.00309
k_2'	0.35310 ±0.01843	0.36191 ±0.03878	0.36687 ±0.06285	0.36943 ±0.06978
k_5	0.05067 ±0.00629	0.05366 ±0.01299	0.05732 ±0.02564	0.05900 ±0.02610
k_6	0.04013 ±0.00935	0.04414 ±0.01770	0.04638 ±0.02974	0.05189 ±0.04647
k_3'	0.02909 ±0.00347	0.02912 ±0.00694	0.02727 ±0.00982	0.02712 ±0.01513
k_5/k_6	1.29869 ±0.16861	1.34984 ±0.46201	1.51485 ±0.69378	1.67803 ±1.21024
K_i	0.00161 ±0.00004	0.00158 ±0.00019	0.00154 ±0.00023	0.00146 ±0.00043

In order to determine the accuracy required in the V_e estimation, we performed a series of experiments, deliberately using incorrect V_e values. A V_e value of 0.16 was used to generate data, which were then analysed assuming V_e values with errors of $\pm 5\%$, $\pm 10\%$ and $\pm 20\%$. One hundred noise-realisations were generated with the 2nd of the 4 noise-levels mentioned above, and mean and SD values were calculated for the estimated parameters across noise-realisations.

IV. RESULTS

The results from the simulations with $V_e = 0.08$, obtained with the 2TC3k and the unconstrained and constrained 3TC5k model, are presented in Tables III–V for basal conditions, and in Tables VI–VIII for insulin stimulated conditions.

For K_1, the 2TC3k model gives biased results, both under basal and insulin stimulated conditions. The 3TC5k model gives accurate K_1-estimates, both with and without constraint, under basal conditions, while under insulin stimulated conditions, the constrained model gives better accuracy and precision, especially at higher noise-levels. The k_2' values are better estimated with the constrained than with the unconstrained 3TC5k model,

TABLE V
ESTIMATED VALUES (mean ± SD) FOR THE CONSTRAINED 3TC5K MODEL WITH $V_e = 0.08$, BASAL CONDITIONS

	Noise level			
	1	*2*	*3*	*4*
K_1	0.02806 ±0.00054	0.02830 ±0.00121	0.02801 ±0.00163	0.02801 ±0.00216
k_2'	0.35077 ±0.00671	0.35370 ±0.01506	0.35012 ±0.02032	0.35016 ±0.02703
k_5	0.04982 ±0.00181	0.05068 ±0.00306	0.05101 ±0.00541	0.05307 ±0.01517
k_6	0.03936 ±0.00473	0.04183 ±0.00827	0.04319 ±0.01519	0.05112 ±0.05413
k_3'	0.02940 ±0.00275	0.03053 ±0.00482	0.03039 ±0.00897	0.03040 ±0.01355
k_5/k_6	1.27901 ±0.11287	1.24319 ±0.16855	1.30030 ±0.41431	1.35317 ±0.50711
K_i	0.00161 ±0.00003	0.00161 ±0.00005	0.00159 ±0.00019	0.00157 ±0.00017

TABLE VI
ESTIMATED VALUES (mean ± SD) FOR THE 2TC3K MODEL WITH $V_e = 0.08$, INSULIN STIMULATED CONDITIONS

	Noise level			
	1	*2*	*3*	*4*
K_1	0.02154 ±0.00065	0.02154 ±0.00119	0.02196 ±0.00191	0.02171 ±0.00296
k_2	0.17303 ±0.00980	0.17251 ±0.01727	0.17932 ±0.02881	0.17708 ±0.04259
k_3	0.07269 ±0.00147	0.07236 ±0.00254	0.07320 ±0.00436	0.07310 ±0.00618
K_i	0.00637 ±0.00002	0.00637 ±0.00003	0.00638 ±0.00005	0.00638 ±0.00008

TABLE VII
ESTIMATED VALUES (mean ± SD) FOR THE UNCONSTRAINED 3TC5K MODEL WITH $V_e = 0.08$, INSULIN STIMULATED CONDITIONS

	Noise level			
	1	*2*	*3*	*4*
K_1	0.02792 ±0.00122	0.02838 ±0.00252	0.02988 ±0.00506	0.03018 ±0.00931
k_2'	0.34886 ±0.03491	0.36690 ±0.08479	0.41804 ±0.18037	0.49186 ±0.60017
k_5	0.14988 ±0.01686	0.15906 ±0.04279	0.17851 ±0.08392	0.21010 ±0.20827
k_6	0.02993 ±0.00894	0.03380 ±0.01950	0.04166 ±0.03877	0.04849 ±0.05798
k_3'	0.05892 ±0.00804	0.05854 ±0.01556	0.05612 ±0.02591	0.05588 ±0.03266
k_5/k_6	5.30595 ±1.11817	5.77738 ±2.43204	7.89498 ±6.84912	10.0904 ±11.0904
K_i	0.00622 ±0.00004	0.00620 ±0.00008	0.00594 ±0.00123	0.00574 ±0.00152

TABLE VIII
ESTIMATED VALUES (mean ± SD) FOR THE CONSTRAINED 3TC5K MODEL WITH $V_e = 0.08$, INSULIN STIMULATED CONDITIONS

	Noise level			
	1	*2*	*3*	*4*
K_1	0.02794 ±0.00074	0.02795 ±0.00134	0.02827 ±0.00208	0.02753 ±0.00340
k_2'	0.34929 ±0.00921	0.34935 ±0.01680	0.35339 ±0.02606	0.34411 ±0.04247
k_5	0.15057 ±0.00584	0.15278 ±0.01072	0.15380 ±0.02132	0.17178 ±0.07150
k_6	0.03060 ±0.00599	0.03327 ±0.01215	0.03625 ±0.02307	0.06667 ±0.15767
k_3'	0.06014 ±0.00682	0.06152 ±0.01364	0.06219 ±0.02314	0.06881 ±0.03806
k_5/k_6	5.06909 ±0.79241	5.08602 ±1.54515	5.76644 ±3.10696	6.00358 ±4.88915
K_i	0.00622 ±0.00003	0.00621 ±0.00007	0.00620 ±0.00016	0.00612 ±0.00065

especially under insulin stimulated conditions, where the unconstrained model results in large bias and variance.

The k_5 and k_6 parameters are slightly better estimated with the constrained than with the unconstrained 3TC5k model. However, the constrained model gives a clearly better estimation of the ratio k_5/k_6, especially under insulin stimulated conditions. This ratio is more important than the individual rate constants, as it determines the steady state concentration-ratio of free tracer in the EES and ICS.

In terms of k_3', the constrained 3TC5k model gives slightly better accuracy than the unconstrained model. The K_i values obtained with the 2TC3k model are biased, especially under basal conditions. The 3TC5k model gives more accurate K_i estimates, with better accuracy and precision in the constrained than in the unconstrained case.

Fig. 6 shows the estimated k_3 and k_3'' values for the 3 different V_e values, normalized to the true k_3'' values. It can be seen that, with the standard 2TC3k model, the estimated k_3 values are close to the true k_3'' values for large V_e values under basal conditions. Otherwise the estimated values are lower. With the unconstrained 3TC5k model, the estimated k_3'' values show large bias and variance. The constrained 3TC5k model, on the other hand, gives much better k_3'' estimates, under both basal and insulin stimulated conditions, although bias and variance increase at higher noise levels. The average coefficient of variation of k_3'' was reduced from 52% to 9.7% by using the V_e constraint, while for k_3 it was 3.4%.

Results from the error estimation experiment are presented in Fig. 7 for K_1 and k_3''. It can be seen that errors in V_e leads to errors in both parameters, although especially in k_3''. Interestingly, the effect on K_i is a combination of the two.

V. DISCUSSION & CONCLUSIONS

In this paper we have proposed a novel approach for kinetic modeling of dynamic PET by incorporation of data derived from DCE-MRI. This allows for an increased complexity in the PET

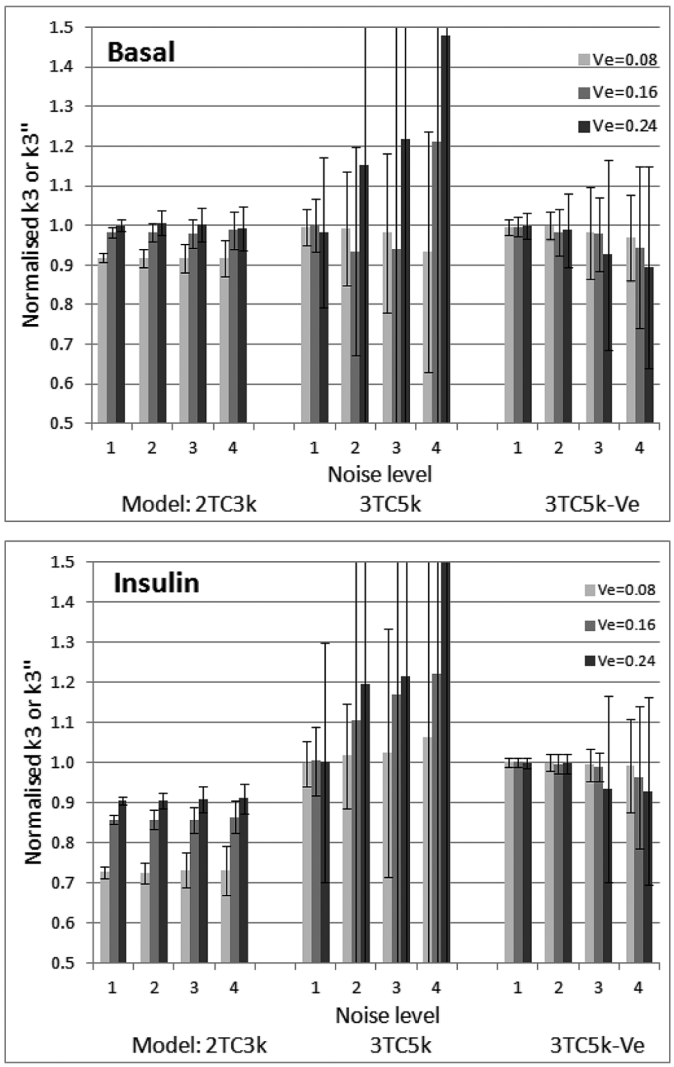

Fig. 6. Estimated values for k_3 or k_3'', normalised to the true k_3'' values (mean $\pm$ SD), for simulations with different V_e-values; including k_3-values from the 2TC3k-model, and k_{3e}''-values from the 3TC5k model unconstrained and constrained (3TC5k-V_e). Results are shown for 4 different noise-levels, for basal (top graph) and insulin stimulated conditions (bottom graph).

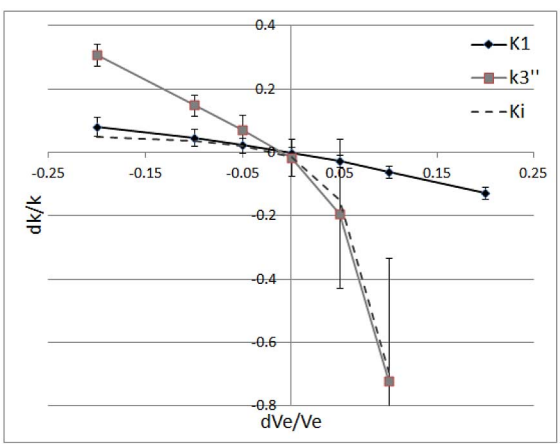

Fig. 7. Estimated relative error in K_1 and k_3'' as a function of the relative error in V_e.

model, possibly providing more specific biological information. The key to this approach is the parameter V_e.

The main outcome measure in [^{18}F]2-FDG kinetic analysis is usually MR_{glu}, which can be calculated based on the macro-parameter K_i, which reflects the combined effects of delivery, transport and phosphorylation of glucose. A change in K_i between 2 scans does not tell you in which of the 3 steps the change occurred. In some cases, however, it may be of interest to be able to distinguish between the different steps in the glucose metabolism [9]–[11]. E.g. the rate of glucose transport across the cellular membrane in skeletal muscle can change under the influence of insulin [11]. Although it may still be difficult to obtain good estimates of the parameters directly related to the transport step (k_5 and k_6), we have shown that our new modeling approach allows for accurate estimation of the parameter k_3'', which reflects the combined effect of transport and phosphorylation. This parameter is similar to k_3 in the standard 2TC3k model, although more specific, since the 3TC5k model includes a distinction between EES and ICS. We have shown that estimated k_3 values can in some cases be close to k_3'', but are not so in general.

The simulations are based on a number of assumptions. Future work will include validation of these assumptions using real data. The advantages of simulated data are that it allows for comparison of the results with the true values and it also enables performing multiple experiments in order to determine the uncertainty in the estimated values.

Using simulated data, we have showed that, if V_e can be accurately derived from DCE-MRI, this parameter can be used as a constraint in a 3TC5k model for [^{18}F]2-FDG in skeletal muscle, resulting in greater accuracy and precision of the estimated parameters as compared to the unconstrained modeling approach. This method could also be used with other tracers, e.g. [^{18}F]FLT, where it could be more beneficial.

REFERENCES

[1] R. E. Carson, "Tracer kinetic modeling in PET," in *Positron Emission Tomography*, D. L. Bailey, P. E. Valk, and M. N. Maisey, Eds. London, U.K.: Springer-Verlag, 2005, pp. 127–159.

[2] R. N. Gunn, S. R. Gunn, and V. J. Cunningham, "Positron emission tomography compartmental models," *J. Cereb. Blood Flow Metab.*, vol. 21, pp. 635–52, Jun. 2001.

[3] M. Ichise, J. H. Meyer, and Y. Yonekura, "An introduction to PET and SPECT neuroreceptor quantification models," *J. Nucl. Med.*, vol. 42, pp. 755–63, May 2001.

[4] K. Erlandsson, "Tracer kinetic modeling: Basics and concepts," in *Basic Sciences of Nuclear Medicine*, M. M. Khalil, Ed. Heidelberg, Germany: Springer, 2011, pp. 333–351.

[5] L. Sokoloff, M. Reivich, C. Kennedy, M. H. Des Rosiers, C. S. Patlak, and K. D. Pettigrew *et al.*, "The [14C]deoxyglucose method for the measurement of local cerebral glucose utilization: Theory, procedure, and normal values in the conscious and anesthetized albino rat," *J. Neurochem.*, vol. 28, pp. 897–916, May 1977.

[6] M. E. Phelps, S. C. Huang, E. J. Hoffman, C. Selin, L. Sokoloff, and D. E. Kuhl, "Tomographic measurement of local cerebral glucose metabolic rate in humans with (F-18)2-fluoro-2-deoxy-D-glucose: Validation of method," *Ann. Neurol.*, vol. 6, pp. 371–88, Nov. 1979.

[7] B. J. Pichler, A. Kolb, T. Nagele, and H. P. Schlemmer, "PET/MRI: Paving the way for the next generation of clinical multimodality imaging applications," *J. Nucl. Med.*, vol. 51, pp. 333–6, Mar. 2010.

[8] P. S. Tofts, G. Brix, D. L. Buckley, J. L. Evelhoch, E. Henderson, and M. V. Knopp *et al.*, "Estimating kinetic parameters from dynamic contrast-enhanced T(1)-weighted MRI of a diffusable tracer: Standardized quantities and symbols," *J. Magn. Reson. Imaging*, vol. 10, pp. 223–32, 1999.

[9] H. M. Huang, F. Ismail-Beigi, and R. F. Muzic, Jr., "A new Michaelis-Menten-based kinetic model for transport and phosphorylation of glucose and its analogs in skeletal muscle," *Med. Phys.*, vol. 38, pp. 4587–99, 2011.

[10] A. Bertoldo, P. Peltoniemi, V. Oikonen, J. Knuuti, P. Nuutila, and C. Cobelli, "Kinetic modeling of [(18)F]FDG in skeletal muscle by PET: A four-compartment five-rate-constant model," *Amer. J. Physiol. Endocrinol. Metab.*, vol. 281, pp. E524–36, Sep. 2001.

[11] A. Bertoldo, R. R. Pencek, K. Azuma, J. C. Price, C. Kelley, and C. Cobelli *et al.*, "Interactions between delivery, transport, and phosphorylation of glucose in governing uptake into human skeletal muscle," *Diabetes*, vol. 55, pp. 3028–37, Nov. 2006.

[12] X. Zhang, Y. Petibon, A. Sitek, K. Takahashi, N. Alpert, and G. El Fakhri *et al.*, "In-vivo Simultaneous DCE-MRI/O-15-water-PET," *J. Nucl. Med.*, vol. 56, p. 644, 2015.

[13] R. B. Innis, V. J. Cunningham, J. Delforge, M. Fujita, A. Gjedde, and R. N. Gunn *et al.*, "Consensus nomenclature for in vivo imaging of reversibly binding radioligands," *J. Cereb. Blood Flow Metab.*, vol. 27, pp. 1533–9, Sep. 2007.

[14] R. F. Muzic, Jr. and S. Cornelius, "COMKAT: Compartment model kinetic analysis tool," *J. Nucl. Med.*, vol. 42, pp. 636–45, Apr. 2001.